

Desmoplakin assembly dynamics in four dimensions: multiple phases differentially regulated by intermediate filaments and actin

Lisa M. Godsel,¹ Sherry N. Hsieh,¹ Evangeline V. Amargo,¹ Amanda E. Bass,¹ Lauren T. Pascoe-McGillicuddy,^{1,4} Arthur C. Huen,¹ Meghan E. Thorne,¹ Claire A. Gaudry,¹ Jung K. Park,¹ Kyunghee Myung,³ Robert D. Goldman,^{3,4} Teng-Leong Chew,³ and Kathleen J. Green^{1,2}

¹Department of Pathology, ²Department of Dermatology, ³Department of Cell and Molecular Biology, and ⁴The R.H. Lurie Cancer Center, Northwestern University Feinberg School of Medicine, Chicago, IL 60611

The intermediate filament (IF)-binding protein desmoplakin (DP) is essential for desmosome function and tissue integrity, but its role in junction assembly is poorly understood. Using time-lapse imaging, we show that cell-cell contact triggers three temporally overlapping phases of DP-GFP dynamics: (1) the de novo appearance of punctate fluorescence at new contact zones after as little as 3 min; (2) the coalescence of DP and the armadillo protein plakophilin 2 into discrete cytoplasmic particles after as little as 15 min; and (3) the cytochalasin-

sensitive translocation of cytoplasmic particles to maturing borders, with kinetics ranging from 0.002 to 0.04 $\mu\text{m/s}$. DP mutants that abrogate or enhance association with IFs exhibit delayed incorporation into junctions, altering particle trajectory or increasing particle pause times, respectively. Our data are consistent with the idea that DP assembles into nascent junctions from both diffusible and particulate pools in a temporally overlapping series of events triggered by cell-cell contact and regulated by actin and DP-IF interactions.

Introduction

Desmosomes are intercellular adhesive junctions that anchor the intermediate filament (IF) cytoskeleton to the plasma membrane. A critical role for these junctions in resisting the forces of mechanical stress is supported by the existence of autoimmune and inherited desmosome diseases that result in skin and heart fragility (for review see Godsel et al., 2004). Desmosomes must also be dynamic because their remodeling is essential in wound healing, development, and morphogenesis. However, the mechanisms that regulate the dissolution and assembly of intercellular junctions during these processes are not well understood.

In desmosomes, transmembrane members of the cadherin family, the desmogleins (Dsgs) and desmocollins (Dscs), cooperate to form the adhesive interface (Garrod et al., 2002). Their cytoplasmic tails associate with armadillo proteins,

plakoglobin (Pg), and plakophilins (PKPs 1–3; Schmidt and Jager, 2005). These cytoplasmic plaque proteins interact with the IF-binding protein desmoplakin (DP), which anchors stress-bearing IFs to the desmosomal plaque (for review see Godsel et al., 2004).

DP is an essential component of desmosomes. Severing DP's connection with IFs impairs cell-cell adhesive strength *in vitro* (Bornslaeger et al., 1996; Huen et al., 2002). Furthermore, DP mutations or loss of DP results in skin and heart defects in humans and mice (Armstrong et al., 1999; Whittock et al., 1999; Norgett et al., 2000; Gallicano et al., 2001; Vasioukhin et al., 2001; Alcalai et al., 2003; Rampazzo et al., 2003; Jonkman et al., 2005; for review see Godsel et al., 2004). DP is a member of the plakin family of cytolinkers with an NH₂-terminal plakin domain, which is important for association with the junctional plaque through interactions with Pg and PKPs, and a central α -helical rod domain that is important for homodimerization (for reviews see Godsel et al., 2004; Jefferson et al., 2004). The COOH terminus comprises three plakin repeat domains, a specialized linker, and terminal regulatory regions that cooperate to facilitate association with IFs (Stappenbeck et al., 1993; Kouklis et al., 1994; Meng et al., 1997; Smith and Fuchs, 1998; Choi et al., 2002; Fontao et al., 2003).

Sherry N. Hsieh and Evangeline V. Amargo contributed equally to this paper.

Correspondence to Kathleen J. Green: kgreen@northwestern.edu

Abbreviations used in this paper: ASMDW, application solution multidimensional workstation; DOX, doxycycline; DP, desmoplakin; DPgly, desmoplakin containing a glycine substitution at Ser2849; DPNTP, desmoplakin NH₂-terminal peptide; Dsc, desmocollin; Dsg, desmoglein; IF, intermediate filament; Pg, plakoglobin; PKP, plakophilin.

The online version of this article contains supplemental material.

Previous studies tracked the redistribution and stabilization of desmosomal cadherins and plaque components in response to increased extracellular calcium (Watt et al., 1984; Jones and Goldman, 1985; Matthey and Garrod, 1986a; Penn et al., 1987; Pasdar et al., 1991). Collectively, these studies suggested that desmosomal cadherins and DP exist in separate compartments and are integrated into junctions at the cell surface. However, the existence and nature of cytoplasmic precursors that contain DP is controversial. Some authors reported that DP-containing particles associated with IFs become redistributed to sites of cell–cell contact upon shifting cells from low to normal calcium, paralleling a reduction of cytoplasmic particles (Jones and Goldman, 1985; Pasdar and Nelson, 1988a,b; Pasdar et al., 1991). These observations led authors to hypothesize that the DP particles are desmosomal precursors. However, direct evidence supporting this idea is lacking, and other investigators have suggested that the particles are desmosomal remnants targeted for degradation (Matthey and Garrod, 1986a,b; Duden and Franke, 1988).

Another unresolved question is how the cytoskeleton might regulate desmosome assembly and DP recruitment to contact sites. Some investigators suggested that DP may be delivered to developing contacts on IFs (Jones and Goldman, 1985), whereas others concluded that IFs are not required (Baribault and Oshima, 1991; Bornslaeger et al., 1996; Vasioukhin et al., 2001). Phosphorylation of DP at Ser2849 was shown to impair interactions between the DP COOH terminus and IFs (Stappenbeck et al., 1994; Meng et al., 1997; Fontao et al., 2003); however, its role in DP localization during desmosome assembly is unknown. Likewise, the role of microfilaments in desmosome assembly is poorly understood. Although one study suggested that cytochalasin B inhibits desmosome assembly (Inohara et al., 1990), another suggested that microfilaments are not required for the accumulation of desmosome components but are for their proper organization and stability at the plasma membrane (Pasdar and Li, 1993).

To overcome the limitations inherent in establishing a temporal sequence of events from fixed specimens, we have used GFP-tagged DP to follow the assembly and fate of desmosome precursors in living cells during junction assembly. Our findings support the idea that cell–cell contact triggers a temporally coordinated process beginning with an initial, rapid local assembly phase followed by the assembly and translocation of cytoplasmic particles containing DP and its armadillo protein binding–partner PKP2. DP dynamics during junction assembly are regulated by both DP–IF interactions and actin microfilaments. These mechanisms are likely to play key roles in coordinating desmosome assembly and maturation during the epithelial remodeling that occurs in development and wound healing.

Results

DP-GFP incorporates normally into desmosomes and is present in discrete cytoplasmic particles

To establish the temporal sequence of DP dynamics and fate during desmosome assembly we generated three COOH-termi-

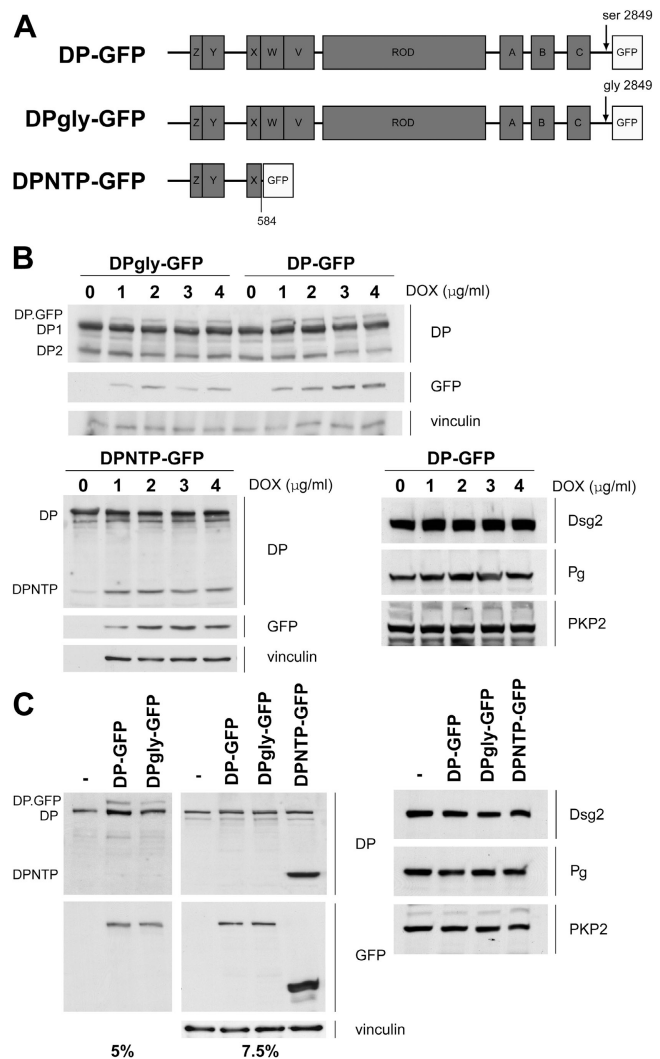


Figure 1. GFP-tagged DP expression and localization. (A) GFP-tagged proteins: full-length DP (DP-GFP) with a wild-type Ser residue at position 2849, a phosphorylation point mutant (DPgly-GFP) with a Ser→Gly replacement at position 2849, and a mutant lacking the central rod and IF-binding domain (DPNTP-GFP). (B) A431 cells were treated with DOX to induce DP-GFP, DPgly-GFP, and DPNTP-GFP, which were expressed at 1/7, 1/13, or 1/4 the level of endogenous DP, respectively. GFP-tagged protein expression did not affect Dsg2, Pg, and PKP2. (C) GFP-tagged and endogenous DP from transiently expressing SCC9 cells were separated on 5 or 7.5% gels. Full-length GFP-tagged proteins (α GFP) were expressed at $\leq 1/5$ the level of endogenous DP. Steady-state levels of endogenous DP, Dsg2, Pg, or PKP2 were not affected compared with parental SCC9s (-). Loading control: α vinculin.

nally tagged DP-GFP constructs: wild-type DP (DP-GFP), a phosphorylation-deficient DP with a Ser→Gly substitution at residue 2849 (DPgly-GFP), and a truncated DP encompassing the NH₂-terminal 584 amino acids (DPNTP-GFP; Fig. 1 A). DPNTP retains the Pg- and PKP-binding domain necessary for incorporation into desmosomes, but lacks the central rod and the COOH-terminal IF-binding domain. The Ser→Gly mutation enhances interactions between the DP COOH terminus and IFs (Stappenbeck et al., 1994; Fontao et al., 2003).

DP-GFP, DPgly-GFP, and DPNTP-GFP were expressed at the predicted molecular weights in inducible A431 (Fig. 1 B)

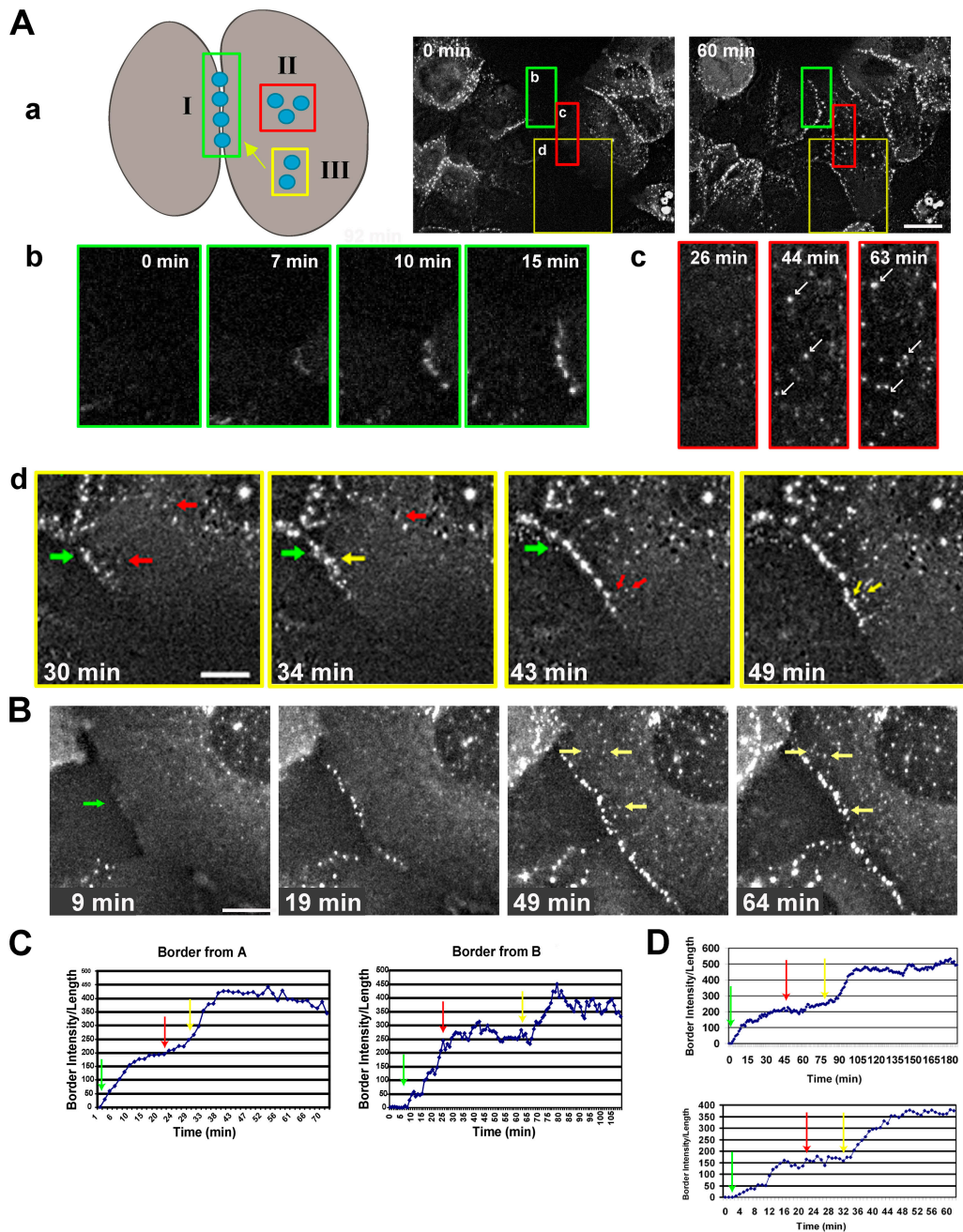
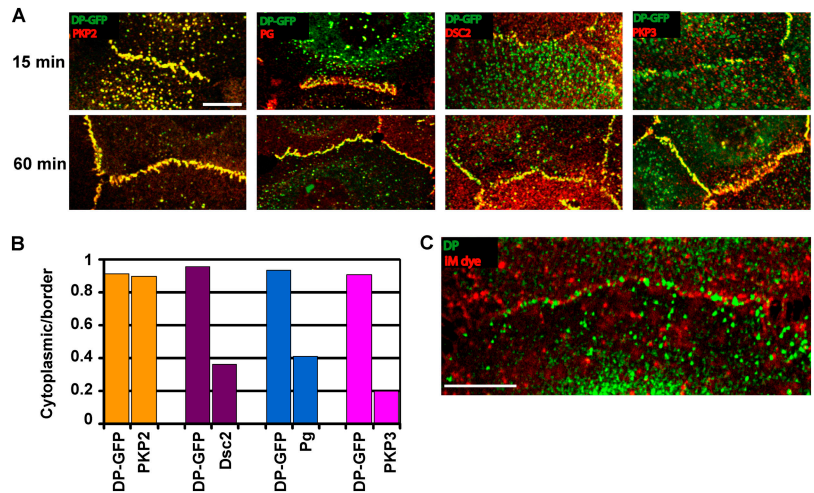


Figure 2. DP accumulation at newly contacting cell-cell borders occurs in three phases. (A) Wounded DP-GFP-expressing A431 monolayers were imaged at 1.5-min intervals. (a) Three phases of DP-GFP dynamics were observed after cell-cell contact. In phase I, fluorescence began to accumulate at sites of contact within ~3–10 min. In phase II, cytoplasmic particles began to appear at 30–45 min of contact. In phase III, cytoplasmic particles moved toward the maturing border. To the right of the schematic are images of the microscopic field at 0 and 60 min after contact. Colored boxes indicate enlarged regions (b–d; Video 1, available at <http://www.jcb.org/cgi/content/full/jcb.200510038/DC1>). Bar, 20 μ m. (b) Phase I: DP appeared within 7 min of cell-cell contact. (c) Phase II: DP dots appeared de novo in the cytoplasm within 25 min of contact. (d) Phase III: Cytoplasmic DP dots moved in an antero-graduate direction and incorporated into the forming border (Video 2). (B) Wounded DP-GFP expressing A431 monolayers were imaged at 1-min intervals (Video 3). The green arrow highlights DP that accumulated within 9 min of cell contact (phase I). Cytoplasmic dots appeared upon initiation of cell contact (49 and 64 min; phase II) and translocated to borders (yellow arrows; phase III). Bar, 10 μ m. Fluorescence intensity over time was calculated for representative borders from the videos in A and B (C) and from 32 other movies (D). In the graphs two waves of border fluorescence corresponded with the onset of phases I (green arrows) and III (yellow arrows). Phase II particle formation occurred at the beginning of or during the plateau between phases I and III (red arrows). Results are representative of data obtained from >50 movies.

and transient SCC9 (Fig. 1 C) transfectants. Full-length GFP-tagged proteins were expressed at only 1/7 to 1/13 of the level of endogenous DP. DPNTP was present at ~1/4 of the level of endogenous DP. Furthermore, the expression level (Fig. 1, B and C) and localization (see Fig. 3) of other desmosomal pro-

teins were not detectably altered. DP-GFP was present in discrete cytoplasmic dots, similar to those previously reported for endogenous DP (Figs. 2–5), and during junction assembly DP-GFP accumulated at borders with a time course comparable to that reported for endogenous protein, where it colocalized in a

Figure 3. PKP2 with DP-GFP colocalize in cytoplasmic particles. (A) DP-GFP-expressing SCC9 cells were fixed at 15 or 60 min after a calcium switch. Confocal imaging demonstrated that DP-GFP colocalized with endogenous PKP2, Pg, Dsc2, and PKP3 at cell borders. DP-GFP cytoplasmic particles near forming borders only infrequently colocalized with Pg, PKP3, or Dsc2, but extensively colocalized with PKP2. Bar, 10 μ m. (B) Average relative fluorescence intensity of each protein in a population of DP-GFP dots, expressed as a ratio with border fluorescence (indicator of maximum colocalization). (C) DP particles did not colocalize with an intracellular membrane dye. Bar, 10 μ m.



typical punctate pattern with other desmosome components (Fig. 2 and Fig. 3; Watt et al., 1984; Jones and Goldman, 1985; Green et al., 1987; Pasdar and Nelson, 1988b).

DP-GFP participates in three temporally overlapping phases of DP dynamics that are triggered by cell-cell contact

To directly examine DP dynamics during desmosome assembly and to address whether DP-containing particles are desmosome precursors, we used time-lapse imaging to follow the fate of DP-GFP in living cells during the process of cell-cell contact formation. In the representative experiments shown in Fig. 2 (A and B), A431 cells inducibly expressing DP-GFP were subjected to light scrape wounding, and z-stacks were collected over time to observe de novo desmosome formation.

Three temporally overlapping phases of DP dynamics were observed (Fig. 2 A, a). First, small fluorescent puncta appeared along the forming border as early as 3 min after cell-cell contact and underwent coalescence and accretion over time (Fig. 2, A [b] and B [green arrows]; and Videos 1–3, available at <http://www.jcb.org/cgi/content/full/jcb.200510038/DC1>). Second, new DP-GFP particles formed in the cytoplasm near newly contacting borders as early as 15 min after cell-cell contact (Fig. 2, A [c and d] and B, arrows; and Videos 1–3, arrows). Third, a subset of preexisting and newly formed particles translocated in an anterograde direction to new contact sites (Fig. 2 A [d] and B; and Videos 1–3). Occasionally, we observed another type of dynamics in which linearly arrayed dots appeared to stream toward remodeling borders (Video 1). Our quantitative analysis focused on particle behavior associated with newly forming contacts (Fig. 2, A [d] and B, yellow arrows; and Videos 2 and 3, yellow arrows). Particles moved with variable kinetics and instantaneous velocities ranging from 0.002 to 0.04 μ m/s. The observed dynamics were independent of differences in DP-GFP expression level, cell background, or clonal variability.

Quantification of fluorescence at newly forming borders over time revealed two waves of increasing intensity that were present in >78% of the 32 borders analyzed (Fig. 2, C and D). The first wave, corresponding to phase I (Fig. 2, C and D, green arrow), was characterized by an ~30–45 min period of

increasing fluorescence. The formation of new cytoplasmic particles (phase II; Fig. 2, C and D, red arrow) was first observed at the beginning or during the plateau that followed. The second wave of intensity corresponded with the onset of particle translocation to borders (phase III; Fig. 2, C and D, yellow arrow). Together, these data support a model in which cell-cell contact triggers three temporally overlapping phases of DP dynamics. These include two productive events that lead to an increase in border fluorescence intensity: a local assembly phase at the membrane, followed by the incorporation of cytoplasmic DP particles.

Assembly-competent DP particles are associated with the armadillo protein PKP2

Toward defining the biochemical nature of DP-containing precursors and the relationship of particle composition to their dynamic behaviors, we performed light and EM analysis of cells undergoing junction assembly. Immunofluorescence analysis of cells after a calcium switch revealed that PKP2 colocalized prominently with particles near nascent junctions (Fig. 3). Two other armadillo family members, PKP3 and Pg, were present in some particles, but not concentrated to the extent of PKP2 (Fig. 3 B). Some larger cytoplasmic structures colocalized with the cadherin Dsc2, but were typically more perinuclear and likely represented engulfed desmosomes. Furthermore, DP-GFP particles close to the zone of cell contact did not colocalize with an intracellular membrane dye, supporting the idea that the precursors are not membrane-bound (Fig. 3 C).

Conventional EM revealed the presence of electron dense particles, similar to those previously reported, associated with IFs and aligned with microfilament bundles (Fig. 4, A and C, arrows). During early stages of assembly, immunogold analysis of whole mount material revealed DP-GFP at cell-cell interfaces in the absence of well-formed plaques and in the cytoplasm close to the zone of contact (Fig. 4, B, D, and G). DP-GFP also localized to desmosomes later in the assembly process (Fig. 4 F). In the cytoplasm, DP-GFP was in clusters of varying sizes and was often associated with IF bundles (Fig. 4, B, D, and F–H). PKP2 also appeared at borders early (Fig. 4 G),

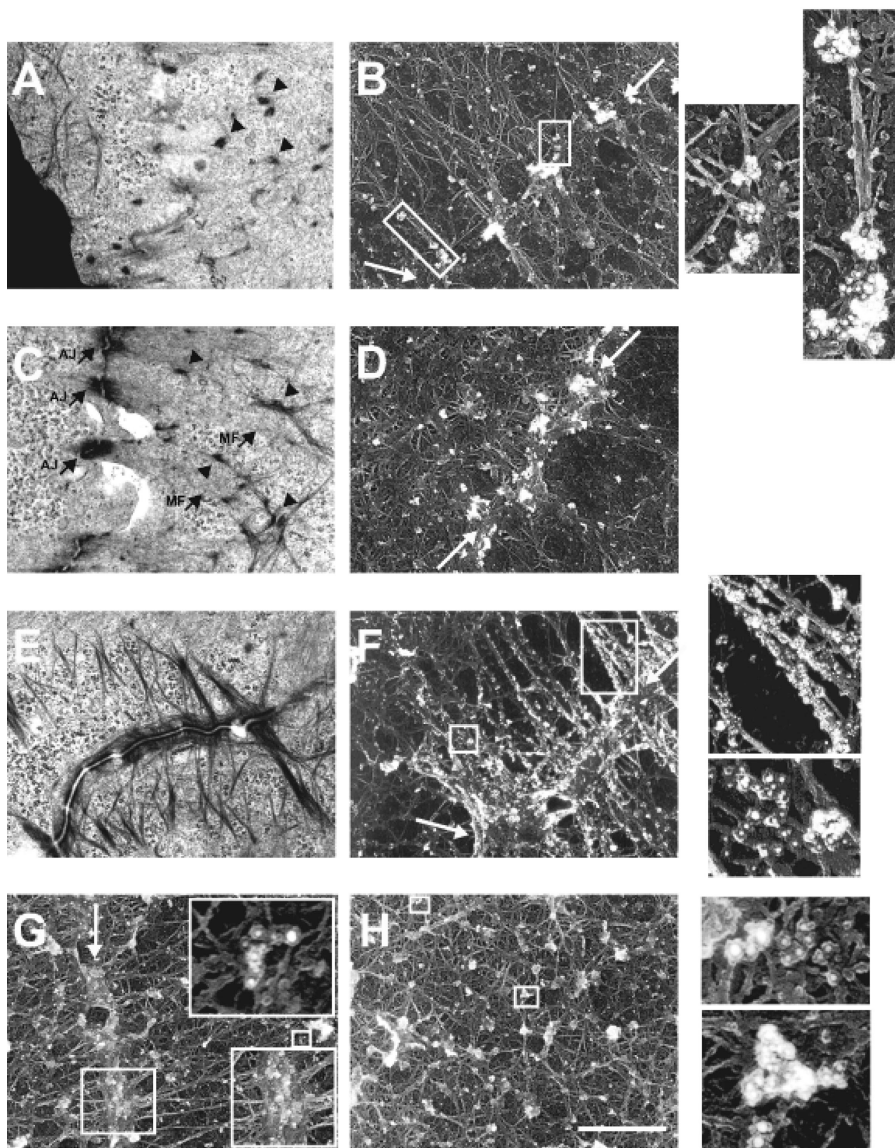


Figure 4. Ultrastructural analysis: DP-GFP associates with nascent junctions, mature desmosomes, and PKP2-containing particles. Conventionally prepared keratinocytes (A, C, and E) and extracted, immunogold-labeled DP-GFP expressing cells (B, D, F, G, and H) were switched from low to normal calcium to induce early cell contacts. (A and C) Conventional EM of contact sites before the appearance of desmosomes. Electron dense, IF-associated cytoplasmic particles were seen in close proximity to microfilaments (MF) near borders (arrowheads) and microfilament-associated adherens junctions (AJ) at contact sites. (B and D) IF and immunogold-labeled DP-GFP at early cell–cell contact sites; white arrows indicate zone of contact. Cytoplasmic DP-GFP particles of varying size were observed near the zone of contact. (E) Conventional EM of a mature desmosome. (F) A mature desmosome with DP-GFP labeling (18-nm gold) at the plaque and along IF bundles labeled for keratin18 (10-nm gold). (G) DP-GFP (10-nm gold) and PKP2 (18-nm gold) at an early border. DP-GFP was observed in association with single or sparse IF at early contact sites (bottom right). (H) DP-GFP (10 nm) and PKP2 (18 nm) colocalized in cytoplasmic particles along IF. Bar, 1 μ m.

later in desmosomes, and in cytoplasmic particles of varying size that colocalized with DP (Fig. 4, G and H). Single or sparsely organized IFs inserted into DP-GFP–positive early contacts (Fig. 4 G, bottom right inset), whereas larger bundles associated with more mature plaques (Fig. 4 F).

To directly correlate particle composition with behavior during junction assembly, we performed retrospective analysis. All phase II DP-GFP particles that appeared during imaging, including those that began to move toward the developing intercellular borders, contained PKP2 (Fig. 5 A and Video 4, available at <http://www.jcb.org/cgi/content/full/jcb.200510038/DC1>), but not Dsc2 (Fig. 5 D and Video 6). Although Pg (Fig. 5 C) and PKP3 (Fig. 5 B and Video 5) were seen in some particles, neither were concentrated to the extent of PKP2 nor was translocation dependent on their presence. In fact, many PKP3- or Dsc2-positive particles were present before cell contact (Fig. 5, B [blue circle] and D [pink circle]) and some moved in a retrograde (Fig. 5 B, orange and yellow ovals) or random (Fig. 5 D, blue circle) motion. Many particles formed

in close association with the keratin IF cytoskeleton (Fig. 5 E), although it was not possible to conclude that all particles formed on IFs. Collectively, these studies demonstrate that DP-GFP selectively assembles with PKP2 into precursor particles during cell contact–initiated desmosome assembly.

Uncoupling DP from IFs or interfering with microfilament organization alters DP particle movement

To test whether loss of the IF-binding domain alters DP dynamics, time-lapse imaging of DPNTF-GFP was performed in cells at the leading edge of a scrape wound. DPNTF-GFP was present in cytoplasmic particles with a wider size range than those assembled from wild-type DP. Furthermore, although $\sim 70\%$ of DP-GFP particles colocalized with keratin IFs, only $\sim 30\%$ of DPNTF-GFP particles colocalized with IF (Fig. 6 A).

Fluorescent DPNTF-GFP puncta appeared at the forming border within 5–10 min of cell–cell contact and underwent coa-

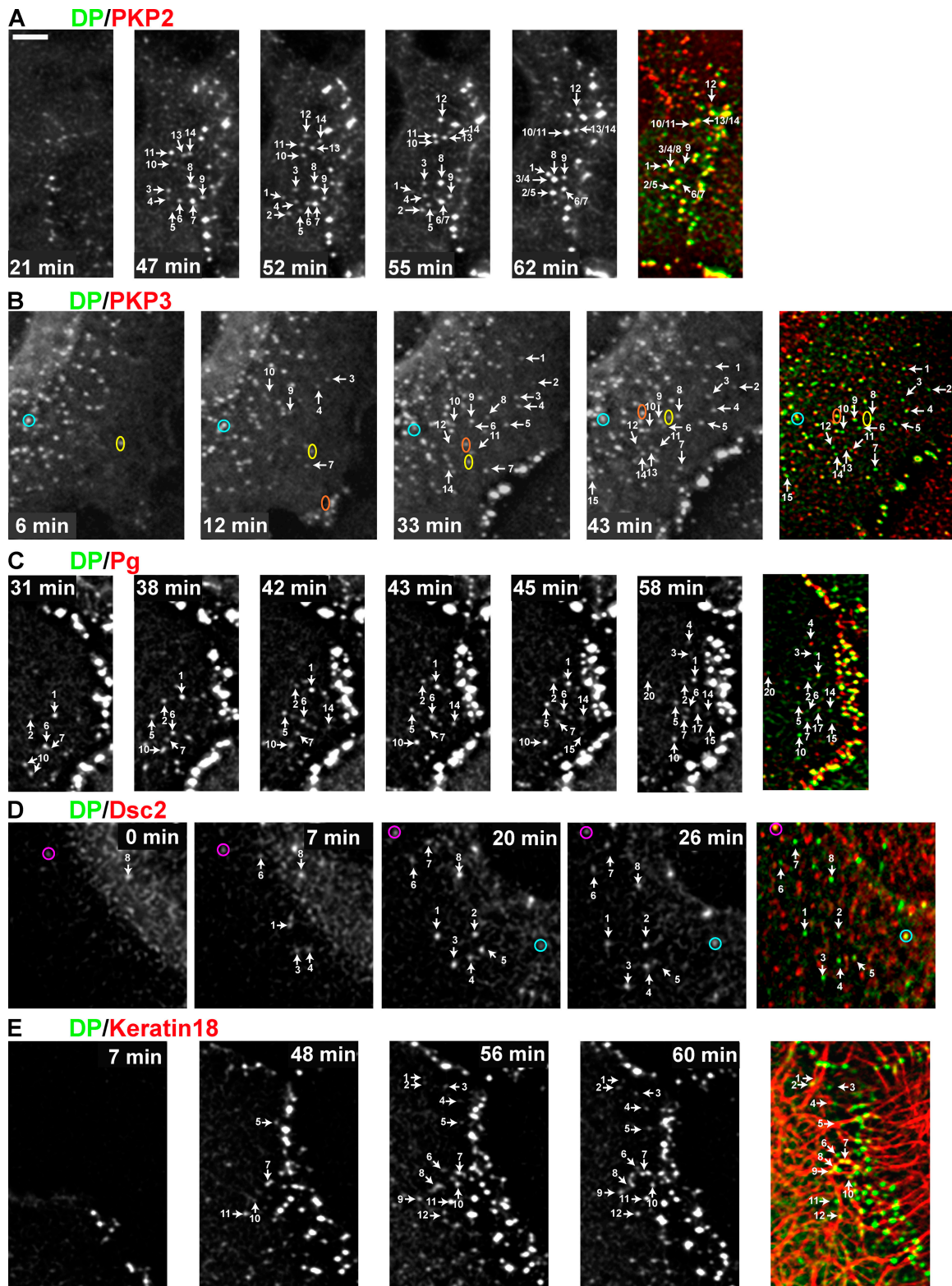


Figure 5. DP-GFP and PKP2 colocalize in the assembly-competent particles that appear after cell-cell contact. Wounded DP-GFP expressing A431 monolayers were imaged at 1-min intervals, fixed, and processed for immunofluorescence after cell-cell contact. (A) PKP2 localizes in all cytoplasmic particles that appeared and moved toward the forming border. Representative images illustrate the fates of numbered DP-GFP particles. Merge shows extensive DP and PKP2 colocalization (Video 4, available at <http://www.jcb.org/cgi/content/full/jcb.200510038/DC1>). (B) Most phase II particles that moved toward the forming border did not contain PKP3 (Video 5). However, many preexisting particles (blue circle) and particles moving in a retrograde fashion (orange and yellow ovals) did colocalize with PKP3. (C) Most phase II particles including those that moved toward the forming border did not contain Pg. (D) Most phase II particles did not contain Dsc2 (Video 6). Dsc2-containing particles were larger, perinuclear, exhibited random movements, and were often present before contact (pink and blue circles). (E) Many phase II DP-GFP containing particles appeared to be associated with IF. Bar, 10 μ m.

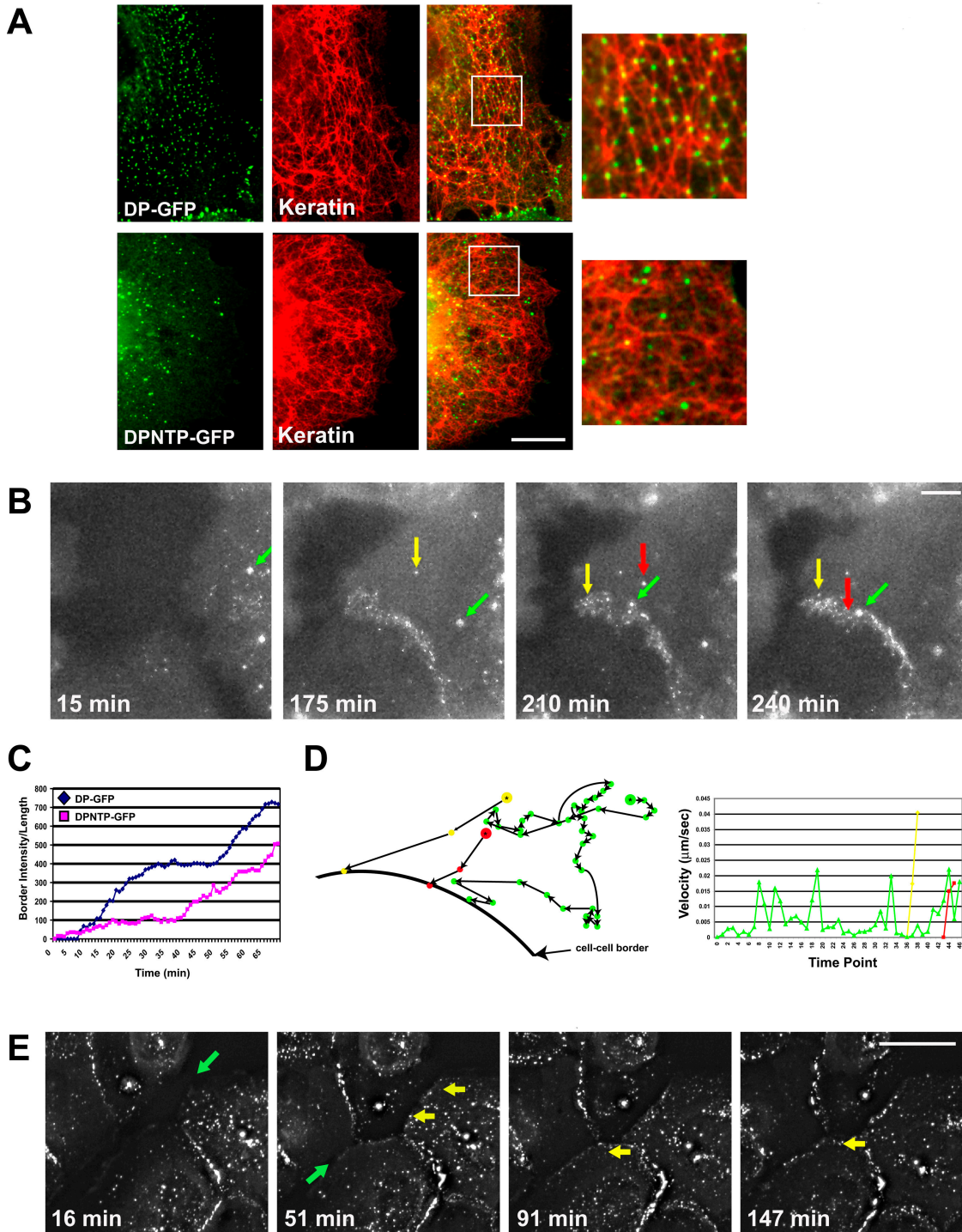
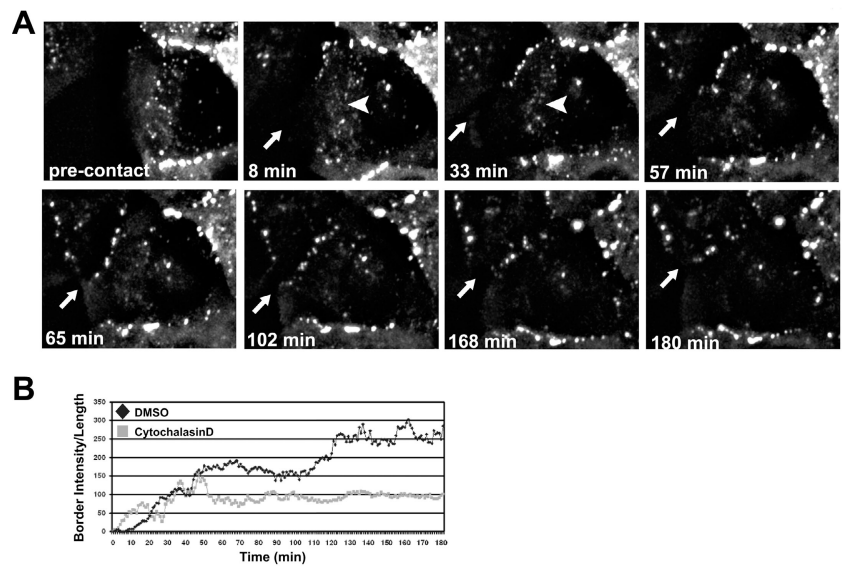


Figure 6. DPNTP-GFP exhibits altered dynamics and delayed junction assembly. (A) DPNTP-GFP does not colocalize with the keratin IF network. DP-GFP or DPNTP-GFP expressing A431 cells (green) were fixed and stained for keratin (red). Although DP-GFP particles aligned with keratin IF, DPNTP-GFP particles were distributed more randomly (see merged and enlarged regions, right). Bar, 10 μm . (B) Wounded DPNTP-GFP expressing A431 monolayers were imaged at 5-min intervals (Video 7, available at <http://www.jcb.org/cgi/content/full/jcb.200510038/DC1>). DPNTP-GFP phase I was comparable to DP-GFP with fluorescence appearing within 5–10 min of contact. Yellow, red, and green arrows follow three DPNTP-containing cytoplasmic phase III particles as they join the forming cell–cell border. Phase II was not observed. Bar, 10 μm . (C) Comparison of DPNTP-GFP (pink squares) and DP-GFP (blue diamonds) fluorescence intensity over time, from paired cells imaged under the same conditions. Although DP-GFP exhibited two waves of border intensity separated by a plateau (Fig. 2), the increase in DPNTP-GFP border fluorescence was more linear with dampened intensity. (D) Schematic depiction of DPNTP-GFP particle trajectory (left) and velocity (right) over time. Colors correspond to the yellow, red, and green arrows designating particles in B. Many particles like the one designated by the green arrow exhibited random movements, traveling a large total distance with fluctuating instantaneous velocities before incorporating. Some particles (yellow and red arrows) exhibited dynamics more similar to DP-GFP, moving directly into the borders without pausing. (E) Wounded DPNTP-GFP expressing A431 were imaged at 1-min intervals (Video 8). Phase I fluorescence appeared within 10 min of contact (green arrow). Phase III particles are marked with yellow arrows. DPNTP-GFP particles exhibited faster, more random dynamics than DP-GFP particles. Bar, 20 μm .

Figure 7. Maturation of DP-GFP borders is cytochalasin D sensitive. (A) Wounded DP-GFP expressing A431 monolayers were imaged at 1-min intervals in the presence of cytochalasin D. Phase I accumulation of DP-GFP (arrows) at the cell–cell border and the formation of phase II particles (arrowheads) was observed in the presence of cytochalasin D. Phase III particle translocation was not observed. (B) Fluorescence border intensity of cytochalasin D treated cells (gray squares) over time was compared with DMSO treated cells imaged in parallel (black diamonds). An initial increase in pixel intensity was observed, but did not increase appreciably over time. A second increase in border fluorescence was not observed, supporting the role of particle translocation in border maturation. Bar, 10 μm .



lescence and accretion over time (Fig. 6, B and E; and Videos 7 and 8, available at <http://www.jcb.org/cgi/content/full/jcb.200510038/DC1>). However, the slope of increased border intensity was dampened (Fig. 6 C). Although some preexisting particles translocated to new contacts, an obvious phase II was not observed. Whereas some particles moved in a directed anterograde fashion, others exhibited random motion before translocating to cell–cell borders (Fig. 6, B, D, and E; and Videos 7 and 8). DPNTP-GFP particles exhibited more rapid movements than DP-GFP particles, reaching instantaneous velocities of 0.08 $\mu\text{m/s}$ compared with 0.04 $\mu\text{m/s}$ for DP-GFP particles. Thus, although IF binding is not required for DP incorporation into desmosomes, DP that lacks the IF binding site interferes with particle assembly, positioning, and dynamics.

Because DP that lacks an IF-binding domain can traffic to intercellular borders, frequently with more rapid kinetics,

and IF-associated DP particles are closely associated with cortical actin (Green et al., 1987), we hypothesized that reorganization of the actin cytoskeleton might drive later phases of DP dynamics. To test this idea, we imaged DP-GFP-expressing cells over time after disrupting filamentous actin with cytochalasin D. Phase I occurred and phase II particles formed (Fig. 7 A and not depicted), but did not appear to translocate to borders (Fig. 7 A). The increase in fluorescence intensity normally associated with phase III was not observed (Fig. 7 B). These data suggest that IFs and microfilaments are both involved in regulating DP dynamics.

DP Ser2849 regulates DP's association with IF and assembly into desmosomes
Abrogation of DP phosphorylation at Ser2849 by site-specific mutation was previously shown to enhance interactions between the

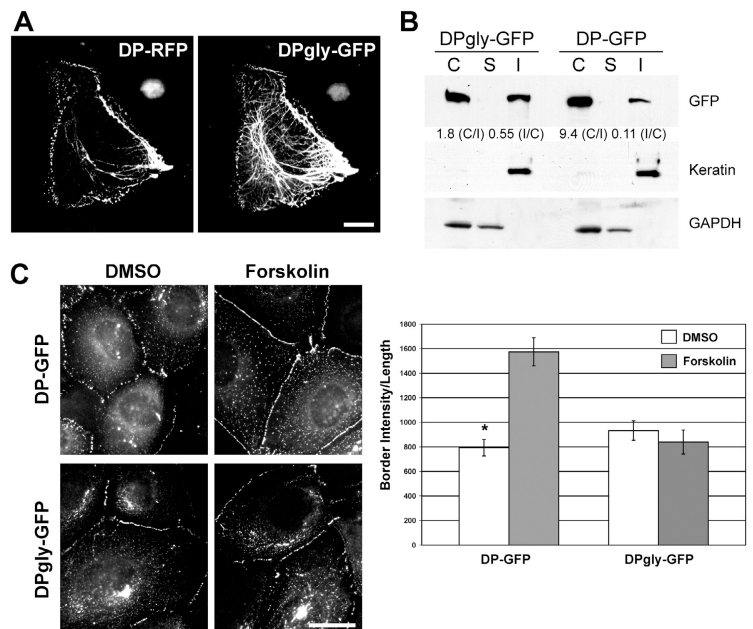


Figure 8. DPgly-GFP associates strongly with IF and is insensitive to forskolin-induced junction recruitment. (A) SCC9 cells were transiently transfected with both full-length DP-RFP and DPgly-GFP. Although DP-RFP was largely at cell borders, DPgly-GFP more prominently decorated IF. Bar, 20 μm . (B) Cells were fractionated into cytoplasmic (C), Triton X-100 soluble (S), and Triton insoluble (I) fractions. DPgly-GFP in the insoluble fraction was 5 \times greater than DP-GFP. (C) SCC9 cells stably expressing DP-GFP or DPgly-GFP were treated with 100 μM forskolin for 16 h. DP-GFP fluorescence increased at cell borders and was more organized with forskolin treatment. No difference in border fluorescence intensity was observed in cells expressing DPgly-GFP. Average fluorescence intensities for a fixed cell population are depicted graphically to the right of representative fluorescence images (*, $P < 0.00001$). Error bars are SEM. Bar, 20 μm .

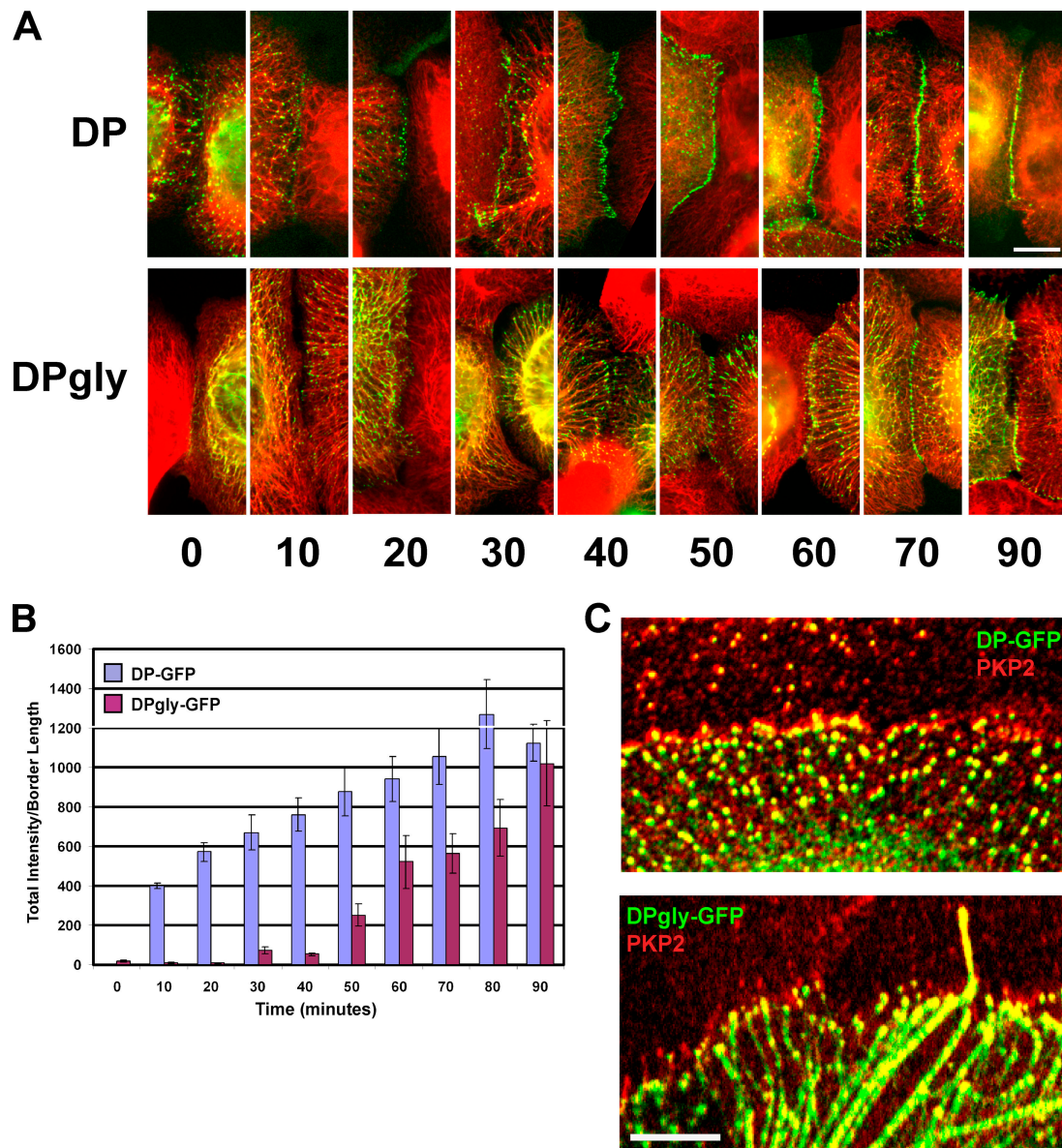


Figure 9. **Assembly of DPgly-GFP into desmosomes after a calcium switch is delayed.** (A) SCC9 cells transiently expressing DP-GFP or DPgly-GFP (green) were fixed at 10-min intervals after a calcium switch (0–90 min) followed by keratin staining (red). DP-GFP appeared at cell borders within 10 min and became prominent by 40 min. DPgly-GFP appeared weakly at cell borders at 20 min, with a dampened increase in intensity at 40 and 60 min. Bar, 10 μ m. (B) Comparison of fluorescence intensities of borders shared by pairs of cells expressing DP-GFP or DPgly-GFP over time. DPgly-GFP exhibited significantly reduced intensities from 10–80 min ($P < 0.03$), normalizing at 90 min. Error bars are SEM. (C) PKP2 colocalized with DP-GFP in cytoplasmic particles and at cell borders (top) and is found in a punctate pattern along filament-associated DPgly-GFP, and at the tips of filament bundles (bottom). Bar, 5 μ m.

DP COOH terminus and IFs (Stappenbeck et al., 1994; Meng et al., 1997; Fontao et al., 2003). To examine the impact of this mutation on full-length DP, the distribution of transiently transfected DP-RFP and the phosphorylation-deficient mutant DPgly-GFP were compared (Fig. 8 A). DPgly-GFP coaligned extensively with IFs, with some punctate staining at borders, whereas DP-RFP was more prominent at cell borders. DP-RFP exhibited some coalignment with IFs, likely because of heterodimerization with DPgly-GFP. The ratio of DPgly-GFP in the detergent insoluble versus cytosolic pool was approximately fivefold greater than that of DP-GFP (Fig. 8 B). These data support the idea that mutation of Ser2849 enhances the association of DP with IF.

We previously demonstrated that activation of PKA using forskolin leads to the phosphorylation of Ser2849, reducing association of the DP COOH terminus with K8/18-rich IF networks (Stappenbeck et al., 1994). We hypothesized that PKA activation might release full-length DP from IFs, thus generating a larger assembly-competent pool. Supporting this idea, fluorescence intensity at borders increased twofold in forskolin-treated DP-GFP, but not DPgly-GFP cells (Fig. 8 C), without altering DP expression (not depicted), consistent with the idea that PKA promotes DP assembly into desmosomes through the phosphorylation of Ser2849. To test whether the phosphorylation-deficient mutant exhibits altered assembly

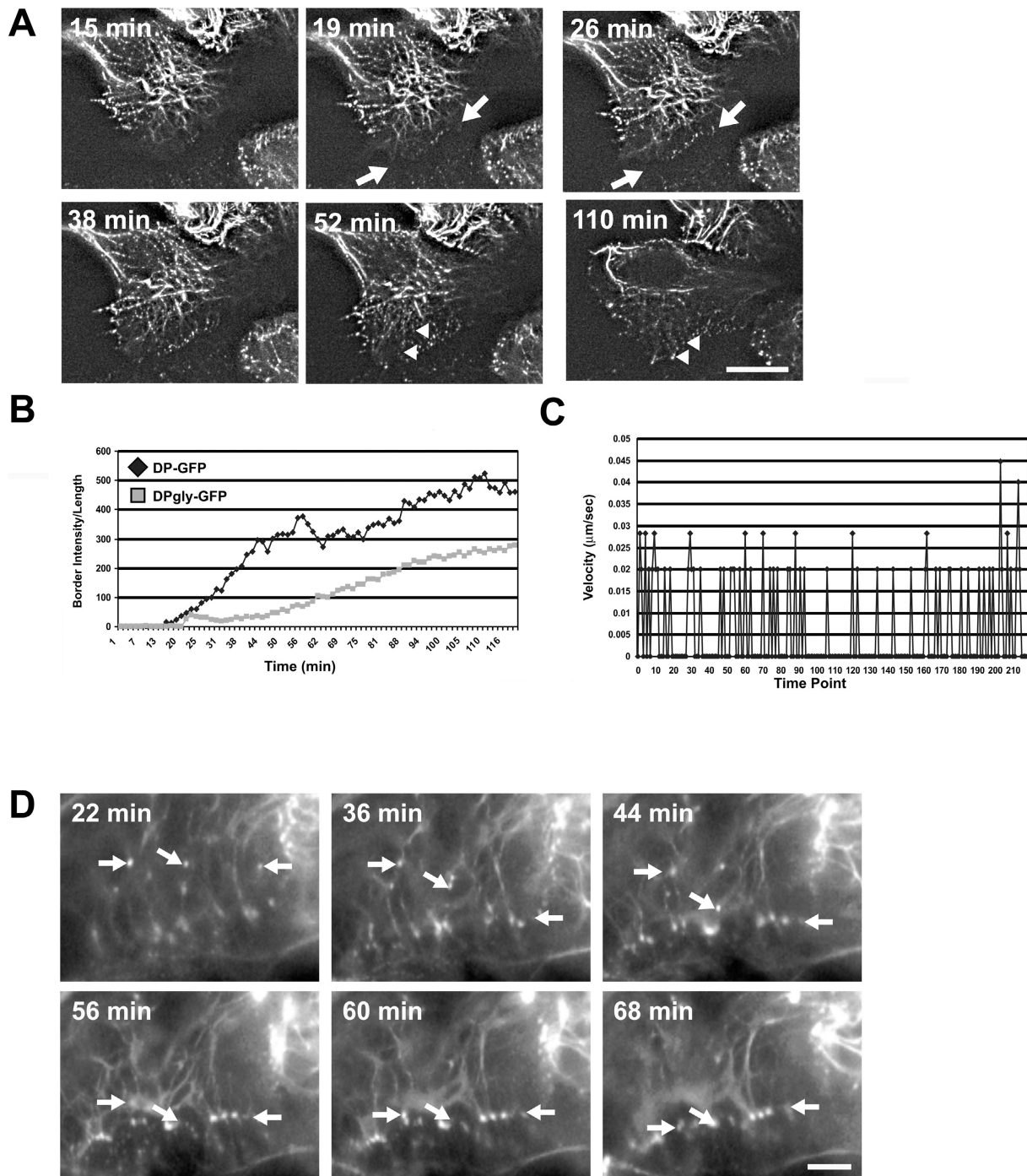


Figure 10. Alterations in DPgly-GFP dynamics impair its incorporation into junctions. (A) Wounded DPgly-GFP-expressing A431 cells were imaged at 15 s intervals (Video 9, available at <http://www.jcb.org/cgi/content/full/jcb.200510038/DC1>). Although all three phases of DP border incorporation were observed, they were temporally delayed. In this movie, phase I (arrows, corresponding to green arrows in Video 9) began after 15 min; the typical onset is 30 min to 1 h after contact. Phase II dots appear to be associated with IF bundles (arrowheads, corresponding to yellow arrows in Video 9). Bar, 20 μ m. (B) Fluorescence intensity comparison of DP-GFP (black diamonds) and DPgly-GFP (gray squares) cells imaged under the same conditions, at the same time. DPgly-GFP border fluorescence was hindered compared with DP-GFP, and the intensity increased in a linear fashion, similar to that observed for DPNTF-GFP (Fig. 6 C). (C) Instantaneous velocities at each time point were calculated for particles from DPgly-GFP-expressing cells. A DPgly-GFP particle displayed fluctuating velocities, with a greater number of pause times (73% of frames during tracking) compared with a DP-GFP particle from a paired movie (33%; not depicted). (D) Phase III dynamics in DPgly-GFP-expressing A431 cells imaged at 2-min intervals (Video 10). IF bundles are decorated by the phosphorylation point mutant and are therefore visible in these cells. Yellow, red, and green arrows follow the dynamics of three DP-containing cytoplasmic particles as they joined the maturing border. Bar, 5 μ m.

kinetics, we calculated fluorescence intensity along contacting borders for pairs of DP-GFP- and DPgly-GFP-expressing cells after a calcium switch (Fig. 9, A and B). Between 10 and 20

min, DP-GFP began to accumulate at cell-cell contact sites, and by 40–50 min border staining was extensive. DPgly-GFP particle redistribution was delayed, with obvious fluorescence

accumulating only after 50–60 min. By 90 min, junction staining normalized, but DPgly-GFP was also retained along cytoplasmic IFs. These results suggest that increased association with the IF cytoskeleton delays DP recruitment to cell–cell contact sites.

As shown in a previous section (Assembly-competent DP particles...), PKP2 is selectively concentrated in DP-GFP precursor particles and its association is correlated with assembly competence. To test whether PKP2's association with DPgly-GFP is altered, we performed confocal colocalization studies. PKP2 colocalized with DPgly-GFP particles and exhibited punctate staining that was overlaid on the continuous DPgly-GFP pattern (Fig. 9 C). These data are consistent with the idea that altered association with IFs, rather than lack of PKP2 association, alters DPgly-GFP assembly kinetics.

DPgly-GFP exhibits altered dynamics and increased pause times during translocation to maturing cell contacts

Analysis of DPgly-GFP by four-dimensional imaging revealed that the average onset of phase I was delayed and fluorescence intensity suppressed, as compared with DP-GFP in cells with continuous staining along IFs (Fig. 10, A and B) and cells with more particulate staining (not depicted). Phase II was either absent or delayed, with phase II particles appearing on DP-coated filaments, which most likely represented keratin bundles (Fig. 10 A and Video 9, available at <http://www.jcb.org/cgi/content/full/jcb.200510038/DC1>). Phase III DPgly-GFP particles exhibited more halting movements and greater pause times than DP-GFP particles (Fig. 10, A, C, and D; and Videos 9 and 10), although instantaneous velocities for DPgly-GFP particles still fell within the range of those exhibited by DP-GFP. A representative particle from Fig. 10 A was stationary from one time point to the next 73% of the time (Fig. 10 C), compared with 33% for a DP-GFP particle from a paired movie (not depicted). 85% of DPgly-GFP particles exhibited pause times, whereas only 30% of DP-GFP particles paused. Collectively, these data suggest that either impairing or enhancing DP–IF interactions delays DP's recruitment to desmosomes.

Discussion

The four-dimensional analyses reported here demonstrate that during desmosome assembly DP-GFP participates in a temporally coordinated process consisting of multiple overlapping components triggered by cell–cell contact. The first response to cell contact is the rapid *de novo* appearance and continuing accretion of fluorescent puncta at new contact sites. DP/PKP2-positive particles then appear in the cytoplasm, some of which are subsequently transported to junctions. The initial, rapid DP accumulation at borders can occur in the absence of the later events, which are sensitive to interference with DP–IF interactions and microfilament organization.

Previous views regarding the origin and fate of cytoplasmic DP-containing particles vary. One view is that particles represent internalized membrane-bound desmosome remnants (Kartenbeck et al., 1982; Matthey and Garrod, 1986b; Duden

and Franke, 1988) not used in future rounds of junction assembly (Matthey and Garrod, 1986b). We do see more perinuclear DP particles colocalizing with desmosomal cadherins, which may be engulfed desmosomes (Fig. 5). We have also observed retrograde flow of DP-GFP originating from cell–cell interfaces, perhaps similar to the irreversible uptake of fluorescent particles observed in cells expressing Dsc2-GFP (Windoffer et al., 2002). This could represent an important mechanism for down-regulating desmosome-mediated adhesion during epithelial remodeling. Those purporting that particles are not precursors have suggested that DP incorporates into desmosomes from a diffusible pool of subunits that assemble *de novo* at cell–cell contact sites (Duden and Franke, 1988). DPI dimers sediment at 6.7-s (O'Keefe et al., 1989) and soluble, possibly oligomeric, 7.3-s and 9-s forms have been reported in epithelial cells (Duden and Franke, 1988; Pasdar and Nelson, 1989). Together with the data presented here, it has been shown soluble DP may provide a pool for the rapid early appearance of DP-GFP at contact sites, as well as a source of DP for phase II particle coalescence.

DP dynamics at the plasma membrane are likely coordinated with the previously reported dynamics of fluorescently labeled desmosomal cadherins (Glouhankova et al., 2003), including the aggregation of assembling Dsc2-GFP puncta (Windoffer et al., 2002). Such a scenario is consistent with immunogold EM analysis showing that Dsg3 is delivered to the plasma membrane into desmosome precursors, some of which are attached to keratin IFs (Sato et al., 2000). DP could coordinate IF attachment to nascent sites of junction assembly, an idea supported by our EM analysis showing DP-GFP associated with sparse IFs at areas of the plasma membrane early in the junction assembly process. The keratin-associated patches of Dsg3 were described as half-desmosome-like clusters, and half desmosomes were previously reported to form at free surfaces in the absence of cell contact (Demlehner et al., 1995; Sato et al., 2000). Although we cannot rule out this type of assembly in our studies, the majority of plasma membrane-associated DP appeared to be at sites of intercellular contact.

Our work also provides compelling evidence to support the model that DP particles are nonmembrane-bound desmosome precursors that become redistributed to the cell periphery after initiation of cell–cell contact (Jones and Goldman, 1985). Nonmembrane-associated DP-GFP particles formed during phase II and translocated into borders. Translocation corresponded temporally with a second increase in fluorescence intensity, which is consistent with the idea that it represents a productive phase of desmosome assembly. Retrospective analysis revealed that PKP2 was present in the assembly-competent particles, suggesting a functional requirement for PKP2 in the formation and/or translocation of these particles. Such a requirement is supported by preliminary RNA interference experiments showing that PKP2 knockdown blocks DP border accumulation (unpublished data). Consistent with the importance of PKP2 for DP plaque association, DP is uncoupled from cardiomyocyte junctions and is present as granular aggregates in the cytoplasm in mice lacking PKP2, leading to defects in heart morphogenesis (Grossmann et al., 2004). Cardiac de-

fects are also seen in humans with PKP2 mutations (Gerull et al., 2004).

The role of PKP2 in DP assembly dynamics is not yet known. PKP family members facilitate DP clustering, which may be important for the accretion of DP during phase I, as well as DP coalescence during phase II. PKP family members associate with both IFs and microfilaments (Hatzfeld et al., 2000; Hofmann et al., 2000), raising the possibility that they may coordinate interactions between DP-GFP particles and the cytoskeleton. Results using cytochalasin D and preliminary data using the myosin II inhibitor blebbistatin (unpublished data) suggest that an actomyosin-based mechanism is required for particle translocation. That the initial local assembly step is not blocked is consistent with the observation that desmosome components accumulated at the membrane of cytochalasin B-treated cells while retaining significant intracellular staining (Pasdar and Li, 1993). The speed of DP particle movement ranges from 0.002 to 0.04 $\mu\text{m/s}$, and is thus slower than that mediated by most conventional motors. DP translocation could be driven indirectly via the redistribution and contraction of the cortical actomyosin ring, known to mature in association with adherens junction formation. Actin may drive the reorganization of DP-associated IF bundles and/or chaperone DP particles to sites of assembly more directly. In the absence of the IF-binding domain, this latter mechanism may proceed more rapidly than when DP is tethered to IF. Consistent with this, instantaneous DPNTF-GFP velocities can reach twice the speed of those observed for DP-GFP. PKP2 in DPNTF particles may coordinate association with actin, thus explaining the ability of untethered particles to reach the plasma membrane.

Although a more definitive analysis of the relationship between DP and IF during assembly awaits dual label imaging studies, our retrospective analysis suggests that many phase II dots form in close association with IF. Furthermore, compromising (DPNTF) or enhancing (DPgly) DP interactions with IFs alters the trafficking patterns and kinetics of DP incorporation into assembling desmosomes. Together, our data support the idea that association with IFs is not required for DP incorporation, but can regulate the course of this process. It is interesting to note that DP particle speeds fall into the same range reported for anterograde keratin particle and keratin “squiggle” movements in keratinocytes (Helfand et al., 2004). Our previous studies suggested that ectopically expressed DP forms oligomeric structures containing IF polypeptides that resemble the desmosomal plaque (Stappenbeck and Green, 1992). Therefore, it seems possible that DP-keratin oligomers may be translocating together to cell-cell borders.

We demonstrate that mutation of Ser2849 leads to an increase in the detergent-insoluble cytoskeletal fraction of DP, consistent with previous findings that PKA-dependent phosphorylation regulates DP-IF binding (Stappenbeck et al., 1994). The delay in phase I/II could thus be explained by a reduction in the availability of diffusible DP due to its sequestration on IF. However, other mechanisms, such as alterations in binding to proteins required for the assembly process, cannot be ruled out. DPgly particles also exhibited greater pause times during translocation, suggesting that junction maturation is altered.

In normal physiological situations, it is probable that desmosome precursor particles comprise a mixture of phosphorylated and unphosphorylated DP. Likewise, due to heterodimerization, it is likely that DPgly-GFP particles contain some endogenous protein. In this way, DPgly-GFP shifts the balance to the less phosphorylated state, allowing us to detect the functional impact of low levels of Ser2849 phosphorylation; i.e., delayed DP recruitment into junctions. Thus Ser2849 phosphorylation may act as a rheostat, regulating precursor recruitment into the plaque, indirectly regulating the rate at which strengthening of desmosome adhesion occurs.

Collectively, these results provide compelling support for the idea that cytoplasmic DP particles can act as junction precursors, but that particle translocation is only one phase of a temporally coordinated process that is regulated by the actin and IF cytoskeletons. The existence of phases with potentially different modes of assembly (e.g., diffusion for phase I not subject to inhibition by cytoskeletal drugs and an actomyosin-dependent mechanism for phase III) could help to reconcile the differing models of desmosome assembly. Regulation of each of these steps is likely to play key roles in regulating the efficiency of desmosome formation during epithelial remodeling that occurs in development and wound healing.

Materials and methods

Generation of constructs

Full-length human DP (DP-GFP; p804) containing the entire coding region (1–8,613 nucleotides) fused to GFP at the COOH terminus was generated by cloning DP into pEGFP-N1 (CLONTECH Laboratories, Inc.), resulting in plasmid p928. To generate the plasmid for use in the doxycycline (DOX)-inducible A431 system, the DP full-length coding region including EGFP was excised from p928 and subcloned into the pTRE2 response plasmid to generate p926. A red fluorescent chimera of DP containing the entire coding region of 1–8,613 nucleotides fused to DsRed2 at the COOH terminus was generated by cloning DP from p928 in pDsRed2-N1 (CLONTECH Laboratories, Inc.), resulting in p991. Full-length DP containing a single Ser→Gly substitution at position 2849 of the protein (DPgly-GFP) was generated by replacing a COOH-terminal fragment in p804 with the same fragment from p86, which harbors a single nucleotide change at position 8,403 to generate p906. To generate the plasmid for use in the Tet-On A431 system (CLONTECH Laboratories, Inc.), the DP-coding region, including EGFP, was excised from p906 and subcloned into the pTRE2 response plasmid to generate p927. Cloning steps for DPNTF-GFP and DPNTF-GFP in the pTRE2 vector are detailed in a previous publication (Huen et al., 2002).

Cell lines, culture conditions, and transfections

SCC9 cell lines (a gift from J. Rheinwald, Harvard Medical School, Boston, MA) were maintained in DME/F-12, 10% FBS, and 1% penicillin/streptomycin. Stable cell lines were maintained in the same culture, with the addition of 400 $\mu\text{g/ml}$ G418. A431-inducible lines were maintained in DME, 10% FBS, 1% penicillin/streptomycin, 400 $\mu\text{g/ml}$ G418, and 1 $\mu\text{g/ml}$ puromycin. Protein expression was induced by culturing the cell lines in 1–4 $\mu\text{g/ml}$ DOX for 24 h. Transient transfections were performed on cultures grown on Type I collagen-coated coverslips (0.1 mg/ml collagen I diluted in 0.02 sodium acetic acid for 1 h at room temperature using the manufacturer's protocol; BD Biosciences) using ExGen 500 according to the manufacturer's protocol (Fermentas Life Sciences). Generation of pTet-On DPNTF-GFP A431 cells was described previously (Huen et al., 2002). DP-GFP and DPgly-GFP were generated as described for DPNTF-GFP cells, screened for expression after 1–4 $\mu\text{g/ml}$ DOX treatment for 24 h, and analyzed by direct fluorescence and immunoblotting. SCC9 stable lines were generated by transfecting cells with either DP-GFP or DPgly-GFP DNA using ExGen 500 transfection reagent (Fermentas Life Sciences) according to the manufacturer's protocol, selected with 400 μg G418, ring cloned, and screened by direct fluorescence and immunoblotting.

Antibodies and reagents

The following primary antibodies were used: Rabbit polyclonals NW161 against the DP NH₂ terminus (Bornslaeger et al., 1996), an anti-EGFP antibody (CLONTECH Laboratories, Inc.), and anti-GAPDH (Novus Biologicals); mouse monoclonals 7G6 against Dsc2, 6D8 against Dsg2, 11E4 against Pg (gifts from M. Wheelock, K. Johnson, and J. Wahl, University of Nebraska Medical Center, Omaha, NE), KSB17.2 against keratin 18 (Sigma-Aldrich), MAB6013S against PKP2 a and b (Marine Biotechnology Services), 23E3 against PKP3 (gift from F. van Roy, VIB-Ghent University, Ghent, Belgium; Bonne et al., 2003), hVIN-1 against vinculin (Sigma-Aldrich), JL-8 against EGFP (CLONTECH Laboratories, Inc.), and a guinea pig polyclonal against PKP2 (gift from W.W. Franke, German Cancer Research Center, Heidelberg, Germany; Mertens et al., 1996). The following secondary antibodies were used: Alexa Fluor 568 goat anti-mouse IgG at 1:300 (Invitrogen), HRP-conjugated goat anti-mouse and goat anti-rabbit IgG at 1:5000 (KLP, Inc.); and 10- or 18-nm colloidal gold-conjugated goat anti-rabbit, 10-nm gold-conjugated goat anti-mouse (Sigma-Aldrich), and 18-nm gold-conjugated donkey anti-guinea pig IgG (Jackson ImmunoResearch Laboratories) at 1:5. The Image-iT LIVE intracellular membrane labeling kit (Invitrogen) was used to stain membranes after fixation following the manufacturer's instructions.

Preparation of cell lysates and immunoblot analysis

Whole cell lysates in Laemmli sample buffer were resolved by 5 or 7.5% SDS-PAGE, and immunoblotted as previously described (Angst et al., 1990), and immunoreactive proteins were visualized using enhanced chemiluminescence. Sequential detergent extractions were performed as described (Palka and Green, 1997). JL-8 (1:1,000), hVIN-1 (1:1,000), 11E4 (1:1,000), 6D8 (1:500), MAB6013 (straight supernatant), KSB17.2 (1:1,000), anti-GAPDH (1:2,000), and NW161 (1:5,000).

Immunofluorescence analysis and image acquisition

Cells were seeded onto collagen-coated glass coverslips and treated with 2–4 µg/ml DOX for 24 h. Coverslips were washed in PBS, fixed in anhydrous methanol for 2 min at –20°C, air dried, and mounted on slides for observation of direct fluorescence or processed for indirect immunofluorescence using KSB17.2 (1:200), 7G6 (1:200), 6D8 (1:50), 11E4 (1:200), 23E3 (1:100), and MAB6013 (undiluted supernatant). Cells incubated with MAB6013 or 23E3 were extracted with 0.5% Triton X-100 for 10 min on ice, after methanol fixation. Primary antibodies were detected using Alexa Fluor 568 goat anti-mouse IgG (Invitrogen) and mounted in polyvinyl alcohol (Sigma-Aldrich). Fixed cells were visualized with a microscope (model DMR; Leica), a confocal microscope (model LSM 510; Carl Zeiss MicroImaging, Inc.), or a spinning disk confocal microscope, consisting of a spinning disc module (Yokogawa Electric) built on an inverted microscope stand (model TE2000U; Nikon) and equipped with a back-thinned charge-coupled device (CCD) camera (Hamamatsu) and illumination by Innova 70 (Laser Innovations) and Omnichrome 500 (Evergreen Laser Corp.) lasers, controlled by an acousto-optical tunable filter. The DMR microscope was fitted with 40× (PL Fluotar, NA 1.0), 63× (PL APO, NA 1.32), and 100× (HCX PLAN APO, NA 1.35) objectives, and images were captured with an Orca 100 CCD camera (model C4742-95; Hamamatsu) and OpenLab 2.2.5 (Improvision) or MetaMorph 6.1 imaging software (Universal Imaging Corp.). Images captured with the LSM 510 microscope were taken using the 100× objective (PLAN APO CHROMAT, NA 1.4) and LSM 510 software. Images captured with the spinning disk confocal microscope were taken with the 100× objective (PLAN APO, NA 1.45) and MetaMorph 6.2.3 software. Images were further processed using Photoshop CS and compiled using Illustrator 9.0.1 or CS (Adobe).

Ultrastructural analysis

Conventional EM of primary mouse keratinocytes was performed as described previously (Starger et al., 1978; Jones and Goldman, 1985; Green et al., 1987). Immunogold labeling was performed for EM using cytoskeletal preparations of SCC9 cells constitutively expressing DP-GFP or DPgly-GFP as previously described (Svitkina and Borisy, 1998) with the following exceptions. Cells were lysed in PEM buffer (100 mM Pipes, pH 6.9, 1 mM MgCl₂, and 1 mM EGTA) containing 1% Triton X-100 and 4% polyethylene glycol. Gelsolin was used to remove actin and microtubules were not preserved. Preparations were examined with a transmission electron microscope (model 100CX; JEOL). Negatives were scanned using the UMAX 1100 and MagicScan32 v4.5 (Umax Data Systems, Inc.) software and processed using Photoshop CS and Illustrator 9.0.1 or CS.

Calcium switch and forskolin and cytochalasin D treatments

SCC9 cells expressing GFP-tagged DP proteins or primary mouse keratinocytes were incubated in low calcium medium (DME with 0.05 mM CaCl₂) for 16 h, switched to normal growth media containing ~1.2 mM Ca²⁺ to induce cell junction assembly for time periods ranging up to 3 h, and processed for immunofluorescence or ultrastructural analysis. For forskolin experiments, SCC9 stable lines were incubated with 100 µM forskolin (Sigma-Aldrich) for 16 h at 37°C. For cytochalasin D time-lapse imaging experiments, wounded monolayers were incubated with 0.3 µg/ml cytochalasin (Calbiochem) or the DMSO carrier and imaged for 230 min.

Time-lapse imaging and retrospective immunofluorescence of DP-GFP particles during junction assembly

Cells were seeded onto 40-mm-diam glass coverslips or Lab-Tek chambered coverglass slides (Nunc) coated with 0.1 mg/ml collagen I, as described in Cell lines, culture conditions, and transfections, and grown to confluence. Monolayers were wounded with small, random holes using a 26-gauge needle and placed at 37°C for 60 min before mounting coverslips into the FCS2 live-cell imaging chamber (Bioptechs, Inc.) or placing chambered slides directly onto the stage. The cell chamber was filled with imaging media (Hanks balanced salt solution, 20 mM Hepes, 1% FBS, 2 mM L-glutamine, 4.5 g/L glucose, 1× amino acids; recipe courtesy of G. Kreitzer, Weill Medical College of Cornell University, New York, NY). Fluorescence and differential interference contrast or phase time-lapse recordings were obtained at 63× (PL APO, NA 1.3) using mercury or halogen illumination with an inverted microscope (model DMIRBE; Leica) fitted with an Orca 100 CCD camera and OpenLab 2.2.5 software or the Application Solution Multidimensional Workstation (ASMDW; Leica) at consistent time intervals of 15 s to 5 min. Images were processed using Photoshop 6.0 and assembled using Adobe Premier or ASMDW software and MetaMorph 6.1 imaging software (Universal Imaging Corp.). The ASMDW contains a DMIRE2 inverted microscope fitted with a Coolsnap HQ (Roper Scientific) camera, a high-precision scanning stage for simultaneous collection of several fields, and a 63× (HCX PL APO, glycerine, NA 1.3) objective fitted with a piezo element for rapid collection of z-stacks (13–15; 0.4–0.5-µm stacks per time point) in a 37°C climate chamber. For retrospective analysis, monolayers were fixed at various times after the observation of cell–cell contact during time lapse imaging and indirect immunofluorescence analysis performed as described in Immunofluorescence analysis and image acquisition. Imaged cells were relocated and z-stacks captured with the ASMDW at 63×. All images obtained with the ASMDW were processed and deconvolved using a blind deconvolution synthetic algorithm, and z-stacks from each time point were assembled into multi-image projections using system software.

Fluorescence intensity of cytoplasmic particles and cell–cell borders, particle kinetics, and densitometric analysis of immunoblots

Fluorescence pixel intensity at cell borders over time was determined by multiplying the average pixel intensity by the area of the defined border divided by the border length. Background intensity was subtracted from border intensity. Error bars represent standard error of the mean, and statistical analysis was performed using *t* test. Particle velocity and distance traveled was calculated for DP containing cytoplasmic particles. Average relative fluorescence intensity was determined by dividing integrated pixel intensity of particles in the cytoplasm by integrated pixel intensity of an identically sized region of fluorescence intensity at the cell–cell border. All calculations were performed using OpenLab 2.2.5 or MetaMorph 6.1 imaging software. Densitometric analyses were performed by scanning immunoblots using the UMAX 1100 and MagicScan32 v4.5 software and analyzed using Molecular Analyst software (Bio-Rad Laboratories).

Online supplemental material

Videos 1 and 2 correspond to Fig. 2 A, and Video 3 corresponds to Fig. 2 B. Videos 4, 5, and 6 correspond to Fig. 5 A, B, and D respectively. For Videos 1–6, A431 cells were induced to express DP-GFP with DOX. Videos 7 and 8 correspond to Fig. 6 B and E, respectively, in which A431 cells were induced to express DPNTF-GFP. Videos 9 and 10 correspond to Fig. 10 A and D, respectively, in which A431 cells were induced to express DPgly-GFP. Online supplemental material is available at <http://www.jcb.org/cgi/content/full/jcb.200510038/DC1>.

We would like to thank those who generously contributed reagents, including J. Wahl, W. Franke, K. Johnson, F. van Roy, and M. Wheelock. Thank you to Dr. G. Kreitzer for assistance with imaging techniques and useful discussions and to Dr. A. Telsler for technical assistance with image scanning and figure

arrangement. We thank Drs. A.P. Kowalczyk and S. Getsios for their helpful discussion and critical reading of this manuscript.

This work was supported by National Institutes of Health grants R01 AR43380 and AR41836 and the J.L. Mayberry endowment to K. Green and DE12328 to K.J. Green and R.D. Goldman. L. Godel was supported in part by grant T32 AR07593 and C.A. Gaudry by a Dermatology Foundation Fellowship.

Submitted: 6 October 2005

Accepted: 17 November 2005

References

- Alcalai, R., S. Metzger, S. Rosenheck, V. Meiner, and T. Chajek-Shaul. 2003. A recessive mutation in desmoplakin causes arrhythmogenic right ventricular dysplasia, skin disorder, and woolly hair. *J. Am. Coll. Cardiol.* 42:319–327.
- Angst, B.D., L.A. Nilles, and K.J. Green. 1990. Desmoplakin II expression is not restricted to stratified epithelia. *J. Cell Sci.* 97:247–257.
- Armstrong, D.K., K.E. McKenna, P.E. Purkis, K.J. Green, R.A. Eady, I.M. Leigh, and A.E. Hughes. 1999. Haploinsufficiency of desmoplakin causes a striate subtype of palmoplantar keratoderma. *Hum. Mol. Genet.* 8:143–148.
- Baribault, H., and R.G. Oshima. 1991. Polarized and functional epithelia can form after the targeted inactivation of both mouse keratin 8 alleles. *J. Cell Biol.* 115:1675–1684.
- Bonne, S., B. Gilbert, M. Hatzfeld, X. Chen, K.J. Green, and F. Van Roy. 2003. Defining desmosomal plakophilin-3 interactions. *J. Cell Biol.* 161:403–416.
- Bornslaeger, E.A., C.M. Corcoran, T.S. Stappenbeck, and K.J. Green. 1996. Breaking the connection: displacement of the desmosomal plaque protein desmoplakin from cell–cell interfaces disrupts anchorage of intermediate filament bundles and alters intercellular junction assembly. *J. Cell Biol.* 134:985–1001.
- Choi, H.J., S. Park-Snyder, L.T. Pascoe, K.J. Green, and W.I. Weis. 2002. Structures of two intermediate filament-binding fragments of desmoplakin reveal a unique repeat motif structure. *Nat. Struct. Biol.* 9:612–620.
- Demlehner, M.P., S. Schafer, C. Grund, and W.W. Franke. 1995. Continual assembly of half-desmosomal structures in the absence of cell contacts and their frustrated endocytosis: a coordinated Sisyphus cycle. *J. Cell Biol.* 131:745–760.
- Duden, R., and W.W. Franke. 1988. Organization of desmosomal plaque proteins in cells growing at low calcium concentrations. *J. Cell Biol.* 107:1049–1063.
- Fontao, L., B. Favre, S. Riou, D. Geerts, F. Jaunin, J.-H. Saurat, K.J. Green, A. Sonnenberg, and L. Borradori. 2003. Interaction of the bullous pemphigoid antigen 1 (BP230) and desmoplakin with intermediate filaments is mediated by distinct sequences within their COOH terminus. *Mol. Biol. Cell.* 14:1978–1992.
- Gallicano, G.I., C. Bauer, and E. Fuchs. 2001. Rescuing desmoplakin function in extra-embryonic ectoderm reveals the importance of this protein in embryonic heart, neuroepithelium, skin and vasculature. *Development.* 128:929–941.
- Garrod, D.R., A.J. Merritt, and Z. Nie. 2002. Desmosomal cadherins. *Curr. Opin. Cell Biol.* 14:537–545.
- Gerull, B., A. Heuser, T. Wichter, M. Paul, C.T. Basson, D.A. McDermott, B.B. Lerman, S.M. Markowitz, P.T. Ellinor, C.A. MacRae, et al. 2004. Mutations in the desmosomal protein plakophilin-2 are common in arrhythmogenic right ventricular cardiomyopathy. *Nat. Genet.* 36:1162–1164.
- Gloushankova, N.A., T. Wakatsuki, R.B. Troyanovsky, E. Elson, and S.M. Troyanovsky. 2003. Continual assembly of desmosomes within stable intercellular contacts of epithelial A-431 cells. *Cell Tissue Res.* 314:399–410.
- Godsel, L.M., S. Getsios, A.C. Huen, and K.J. Green. 2004. The molecular composition and function of desmosomes. In *Cell Adhesion*. J.N. Behrens and W.J. Nelson, editors. Springer-Verlag New York, Inc., New York. 137–193.
- Green, K.J., B. Geiger, J.C. Jones, J.C. Talian, and R.D. Goldman. 1987. The relationship between intermediate filaments and microfilaments before and during the formation of desmosomes and adherens-type junctions in mouse epidermal keratinocytes. *J. Cell Biol.* 104:1389–1402.
- Grossmann, K.S., C. Grund, J. Huelsken, M. Behrend, B. Erdmann, W.W. Franke, and W. Birchmeier. 2004. Requirement of plakophilin 2 for heart morphogenesis and cardiac junction formation. *J. Cell Biol.* 167:149–160.
- Hatzfeld, M., C. Haffner, K. Schulze, and U. Vinzens. 2000. The function of plakophilin 1 in desmosome assembly and actin filament organization. *J. Cell Biol.* 149:209–222.
- Helfand, B.T., L. Chang, and R.D. Goldman. 2004. Intermediate filaments are dynamic and motile elements of cellular architecture. *J. Cell Sci.* 117:133–141.
- Hofmann, I., C. Mertens, M. Brettel, V. Nimrich, M. Schnolzer, and H. Herrmann. 2000. Interaction of plakophilins with desmoplakin and intermediate filament proteins: an in vitro analysis. *J. Cell Sci.* 113:2471–2483.
- Huen, A.C., J.K. Park, L.M. Godsel, X. Chen, L.J. Bannon, E.V. Amargo, T.Y. Hudson, A.K. Mongiu, I.M. Leigh, D.P. Kelsell, et al. 2002. Intermediate filament–membrane attachments function synergistically with actin-dependent contacts to regulate intercellular adhesive strength. *J. Cell Biol.* 159:1005–1017.
- Inohara, S., Y. Tatsumi, H. Cho, Y. Tanaka, and S. Sagami. 1990. Actin filament and desmosome formation in cultured human keratinocytes. *Arch. Dermatol. Res.* 282:210–212.
- Jefferson, J.J., C.L. Leung, and R.K. Liem. 2004. Plakins: goliaths that link cell junctions and the cytoskeleton. *Nat. Rev. Mol. Cell Biol.* 5:542–553.
- Jones, J.C., and R.D. Goldman. 1985. Intermediate filaments and the initiation of desmosome assembly. *J. Cell Biol.* 101:506–517.
- Jonkman, M.F., A.M.G. Pasmooij, S.G.M.A. Pasmans, M.P. van den Berg, H.J. ter Horst, A. Timmer, and H.H. Pas. 2005. Loss of desmoplakin tail causes lethal acantholytic epidermolysis bullosa. *Am. J. Hum. Genet.* 77:653–660.
- Kartenbeck, J., E. Schmid, W.W. Franke, and B. Geiger. 1982. Different modes of internalization of proteins associated with adherens junctions and desmosomes: experimental separation of lateral contacts induces endocytosis of desmosomal plaque material. *EMBO J.* 1:725–732.
- Kouklis, P.D., E. Hutton, and E. Fuchs. 1994. Making a connection: direct binding between keratin intermediate filaments and desmosomal proteins. *J. Cell Biol.* 127:1049–1060.
- Mattey, D.L., and D.R. Garrod. 1986a. Calcium-induced desmosome formation in cultured kidney epithelial cells. *J. Cell Sci.* 85:95–111.
- Mattey, D.L., and D.R. Garrod. 1986b. Splitting and internalization of the desmosomes of cultured kidney epithelial cells by reduction in calcium concentration. *J. Cell Sci.* 85:113–124.
- Meng, J.J., E.A. Bornslaeger, K.J. Green, P.M. Steinert, and W. Ip. 1997. Two-hybrid analysis reveals fundamental differences in direct interactions between desmoplakin and cell type-specific intermediate filaments. *J. Biol. Chem.* 272:21495–21503.
- Mertens, C., C. Kuhn, and W.W. Franke. 1996. Plakophilins 2a and 2b: constitutive proteins of dual location in the karyoplasm and the desmosomal plaque. *J. Cell Biol.* 135:1009–1025.
- Norgett, E.E., S.J. Hatsell, L. Carvajal-Huerta, J.C. Cabezas, J. Common, P.E. Purkis, N. Whittock, I.M. Leigh, H.P. Stevens, and D.P. Kelsell. 2000. Recessive mutation in desmoplakin disrupts desmoplakin-intermediate filament interactions and causes dilated cardiomyopathy, woolly hair and keratoderma. *Hum. Mol. Genet.* 9:2761–2766.
- O’Keefe, E.J., H.P. Erickson, and V. Bennett. 1989. Desmoplakin I and desmoplakin II. Purification and characterization. *J. Biol. Chem.* 264:8310–8318.
- Palka, H.L., and K.J. Green. 1997. Roles of plakoglobin end domains in desmosome assembly. *J. Cell Sci.* 110:2359–2371.
- Pasdar, M., and W.J. Nelson. 1988a. Kinetics of desmosome assembly in Madin-Darby canine kidney epithelial cells: temporal and spatial regulation of desmoplakin organization and stabilization upon cell–cell contact. I. Biochemical analysis. *J. Cell Biol.* 106:677–685.
- Pasdar, M., and W.J. Nelson. 1988b. Kinetics of desmosome assembly in Madin-Darby canine kidney epithelial cells: temporal and spatial regulation of desmoplakin organization and stabilization upon cell–cell contact. II. Morphological analysis. *J. Cell Biol.* 106:687–695.
- Pasdar, M., and W.J. Nelson. 1989. Regulation of desmosome assembly in epithelial cells: kinetics of synthesis, transport, and stabilization of desmoglein I, a major protein of the membrane core domain. *J. Cell Biol.* 109:163–177.
- Pasdar, M., and Z. Li. 1993. Disorganization of microfilaments and intermediate filaments interferes with the assembly and stability of desmosomes in MDCK epithelial cells. *Cell Motil. Cytoskeleton.* 26:163–180.
- Pasdar, M., K.A. Krzeminski, and W.J. Nelson. 1991. Regulation of desmosome assembly in MDCK epithelial cells: coordination of membrane core and cytoplasmic plaque domain assembly at the plasma membrane. *J. Cell Biol.* 113:645–655.
- Penn, E.J., I.D. Burdett, C. Hobson, A.I. Magee, and D.A. Rees. 1987. Structure and assembly of desmosome junctions: biosynthesis and turnover of the major desmosome components of Madin-Darby canine kidney cells in low calcium medium. *J. Cell Biol.* 105:2327–2334.
- Rampazzo, A., G. Beggagna, A. Nava, G. Occhi, B. Baucce, M. Noiato, C. Basso, G. Frigo, G. Thiene, J. Towbin, and G.A. Danielli. 2003. Arrhythmogenic right ventricular cardiomyopathy type 1 (ARVD1): confirmation of lo-

- cus assignment and mutation screening of four candidate genes. *Eur. J. Hum. Genet.* 11:69–76.
- Sato, M., Y. Aoyama, and Y. Kitajima. 2000. Assembly pathway of desmoglein 3 to desmosomes and its perturbation by pemphigus vulgaris-IgG in cultured keratinocytes, as revealed by time-lapsed labeling immunoelectron microscopy. *Lab. Invest.* 80:1583–1592.
- Schmidt, A., and S. Jager. 2005. Plakophilins—hard work in the desmosome, recreation in the nucleus? *Eur. J. Cell Biol.* 84:189–204.
- Smith, E.A., and E. Fuchs. 1998. Defining the interactions between intermediate filaments and desmosomes. *J. Cell Biol.* 141:1229–1241.
- Stappenbeck, T.S., and K.J. Green. 1992. The desmoplakin carboxyl terminus coaligns with and specifically disrupts intermediate filament networks when expressed in cultured cells. *J. Cell Biol.* 116:1197–1209.
- Stappenbeck, T.S., E.A. Bornslaeger, C.M. Corcoran, H.H. Luu, M.L. Virata, and K.J. Green. 1993. Functional analysis of desmoplakin domains: specification of the interaction with keratin versus vimentin intermediate filament networks. *J. Cell Biol.* 123:691–705.
- Stappenbeck, T.S., J.A. Lamb, C.M. Corcoran, and K.J. Green. 1994. Phosphorylation of the desmoplakin COOH terminus negatively regulates its interaction with keratin intermediate filament networks. *J. Biol. Chem.* 269:29351–29354.
- Starger, J., W. Brown, A. Goldman, and R. Goldman. 1978. Biochemical and immunological analysis of rapidly purified 10-nm filaments from baby hamster kidney (BHK-21) cells. *J. Cell Biol.* 78:93–109.
- Svitkina, T.M., and G.G. Borisy. 1998. Correlative light and electron microscopy of the cytoskeleton of cultured cells. *Methods Enzymol.* 289:570–592.
- Vasioukhin, V., E. Bowers, C. Bauer, L. Degenstein, and E. Fuchs. 2001. Desmoplakin is essential in epidermal sheet formation. *Nat. Cell Biol.* 3:1076–1085.
- Watt, F.M., D.L. Matthey, and D.R. Garrod. 1984. Calcium-induced reorganization of desmosomal components in cultured human keratinocytes. *J. Cell Biol.* 99:2211–2215.
- Whitlock, N.V., G.H. Ashton, P.J. Dopping-Hepenstal, M.J. Gratian, F.M. Keane, R.A. Eady, and J.A. McGrath. 1999. Striate palmoplantar keratoderma resulting from desmoplakin haploinsufficiency. *J. Invest. Dermatol.* 113:940–946.
- Windoffer, R., M. Borchert-Stuhltrager, and R.E. Leube. 2002. Desmosomes: interconnected calcium-dependent structures of remarkable stability with significant integral membrane protein turnover. *J. Cell Sci.* 115:1717–1732.